Endogenous Dynamic Nuclear Polarization NMR of Hydride-Terminated Silicon Nanoparticles

Michelle Ha[§,1], Alyxandra N. Thiessen[§,1], Ivan V. Sergeyev [2], Jonathan G. C. Veinot [1,], and Vladimir K. Michaelis [1,*]*

[1] Department of Chemistry, University of Alberta, Edmonton, AB, Canada, T6G 2G2

[2] Bruker-Biospin Corporation, 15 Fortune Drive, Billerica, MA, USA, 01821

Author Information

[§]Author Contributions: M.H. and A.N.T. contributed equally to this work.

*Corresponding Authors: vladimir.michaelis@ualberta.ca and jveinot@ualberta.ca

ABSTRACT

Silicon nanoparticles (SiNPs) are intriguing materials and their properties fascinate the broader scientific community; they are also attractive to the biological and materials science sub-disciplines because of their established biological and environmental compatibility as well as their far-reaching practical applications. While characterization of the particle nanostructure can be performed using ^{29}Si solid-state nuclear magnetic resonance (NMR) spectroscopy, poor sensitivity due to low Boltzmann population and long acquisition times hinder in-depth studies of these potentially game-changing materials. In this study, we compare two DNP NMR protocols to boost ^{29}Si sensitivity in hydride-terminated SiNPs. First, we assess a traditional indirect DNP approach, where a nitroxide biradical (AMUPol or bCTbk) is incorporated into a glassing agent and transferred through protons ($e^- \rightarrow {}^1H \rightarrow {}^{29}Si$) to enhance the silicon. In this mode, electron paramagnetic resonance (EPR) spectroscopy demonstrated that the hydride-terminated surface was highly reactive with the exogenous biradicals, thus decomposing the radicals within hours and resulting in an enhancement factor, ε, of 3 (T_B=15 s) for the 64 nm SiNP, revealing the surface components. Secondly, direct DNP NMR methods were used to enhance the silicon without the addition of an exogenous radical (i.e., use of dangling bonds as an endogenous radical source). With radical concentrations < 1 mM, ^{29}Si enhancements were obtained for the series of SiNPs ranging from 3 to 64 nm. The ability to use direct ^{29}Si DNP transfer ($e^- \rightarrow {}^{29}Si$) shows promise for DNP studies of these inorganic nanomaterials (ε = 6 (T_B = 79 min) for 64 nm SiNPs) with highly reactive surfaces, showing the sub-surface and core features. These preliminary findings lay a foundation for future endogenous radical development through tailoring the surface chemistry, targeting further sensitivity gains.

Keywords: DNP NMR, silicon nanoparticles, endogenous, cross effect, field profile

1. INTRODUCTION

Scientific instrumentation and spectroscopic methods have advanced rapidly, making it possible to overcome barriers that have previously limited the characterization, and by extension, the community's understanding of challenging complex biological and energy materials that could revolutionize their respective fields. Solid-state nuclear magnetic resonance (NMR) spectroscopy is among the most powerful non-destructive methods available for characterizing dynamics and atomic-level structure in ordered and disordered solids. Unfortunately, studying nuclear spins often leads to complications related to poor sensitivity, arising from the low Boltzmann polarization, and long acquisition times ranging from hours to days. To circumvent these issues, various approaches, or combinations thereof, have been implemented to improve detection limits and push beyond the status quo. Gains in sensitivity can be achieved via isotopic enrichment or the study of high-γ and highly abundant nuclei (e.g., ^{1}H or ^{19}F) in combination with cross-polarization techniques [1], magic angle spinning (MAS) [2,3], and ultrahigh magnetic fields [4].

High-field dynamic nuclear polarization (DNP) has revolutionized NMR spectroscopy; it is a highly sensitive analytical method that is impacting nearly all fields of chemical research by dramatically and significantly reducing experimental acquisition times and increasing detection limits. These game-changing advancements have been made possible by the large thermal electron spin polarization of a paramagnetic species, achieved by irradiating the sample with high-frequency microwaves, that can then be transferred to surrounding nuclei [5-7]. The gain in sensitivity is often quantified as the DNP enhancement factor (ε) which is the comparison of the signal-to-noise ratio of the microwave-on and -off NMR spectra acquired under identical conditions; the corresponding reduction in experimental time is thus determined by a factor of ε^2 [8]. Often, large gains in sensitivity are achieved using indirect DNP polarization, which is typically accomplished using nitroxide-based biradicals as the electron polarizing agent; examples include TOTAPOL [9],

SPIROPOL [10], AMUPol [11], or TEKPOL [12,13], among many others [14-19]. Upon microwave irradiation, the polarization of unpaired electrons is transferred to the ^{1}H nuclei in the sample of interest, theoretically reaching an enhancement factor of 658 (γ_e/γ_{1H}). The polarization from ^{1}H can then be transferred to other lower-γ nuclei via cross-polarization; this process facilitates the study of a wide scope of biological and inorganic chemical problems [8, 20 22]. Alternatively, electron polarization can be transferred directly to the NMR-active nucleus of interest (direct DNP). In these cases, it is necessary to employ exogenous radicals displaying more effective match conditions; for example, trityl radicals are ideal for polarizing ^{2}H (γ_e/γ_{2H} = 4291) [23], ^{17}O (γ_e/γ_{17O} = 4857) [24], or ^{13}C (γ_e/γ_{13C} = 2616) [25] nuclei with enhancement factors ranging from 100 to greater than 600 (i.e., > 10,000 reduction in the time required to obtain comparable NMR spectra) [26]. Regardless of the polarization transfer mechanism, DNP NMR is a powerful emerging spectroscopic method for the chemical sciences.

To achieve bulk polarization transfer for insulating solids, solid effect (SE) and cross effect (CE) mechanisms are often considered [2732]. For example, wide-line nitroxide radicals are optimal for CE, while narrow-line radicals such as BDPA are more suited for ^{1}H SE. The CE mechanism is often favoured due to its large enhancement factors, the diverse array of commercially available wide-line radicals, less detrimental scaling efficiency with increasing magnetic field strength, and stringent microwave power requirements associated with SE (i.e., forbidden transition) [33].

The study of certain solids may be hampered when using organic biradicals if the radical reacts with the solid of interest (e.g., inducing polymerization or deactivation of the radical) or changes the chemically relevant environment (e.g., binding to a catalytic metal site [34]). To circumvent the need to add an exogenous radical and associated glassing agent(s), various groups have attempted to introduce a paramagnetic center into their chemical system, with the hope of polarizing the nuclei of interest in their solid sample. For example, Mn^{2+} dopants have been successfully used as an

88 endogenous polarizing agent in hammerhead riboyzyme complexes [35], as well as in battery anode
89 materials [36], Griffin and colleagues have successfully polarized ^{1}H, ^{13}C and ^{59}Co using Cr(III) [37],
90 while Shumacher and Slicther used the paramagnetic susceptibility of conduction electron spins for
91 ^{7}Li enhancements in metallic lithium [38]. Along similar lines, Ramanathan *et al.* utilized the unique
92 feature of dangling bonds within Si microparticles (≥ 0.3 μm) to polarize ^{29}Si directly [39], and more
93 recently to investigate the SiO_x/H_2O interface through ^{1}H DNP NMR [40]. In 2008, Ramanathan and
94 colleagues obtained excellent ^{29}Si DNP enhancements and tunable long nuclear spin-lattice relaxation
95 times (T_1) for a series of silicon microparticles ranging in size from ~0.3 to a few μm. Using a
96 combination of low-field DNP NMR (B_0 < 3 T) and ultra-low temperatures (< 30 K), they made use
97 of the endogenous unpaired electrons from dangling bonds within the Si/SiO_x amorphous interface
98 surrounding the crystalline bulk core as the polarizing source [41]. The authors demonstrated the T_1s
99 were sensitive to particle size and that the amorphous SiO_x region made up approximately 20% of the
100 total mass.

101 While most DNP studies have focused on micron-sized silicon particles, there is much interest in
102 analyzing and understanding nanometer-scale particles that lie within the size regime where non-bulk
103 properties emerge. Silicon nanoparticles (SiNPs) with dimensions of 1 to 100 nm hold promise of
104 impacting a wide range of applications including, but not limited to, photovoltaics, thermoelectrics,
105 batteries, and nanomedicine [42,43]. In this context, we build upon previous DNP studies of Si
106 microparticles and explore the effectiveness of exogenous and endogenous radicals for indirect and
107 direct DNP NMR of well-defined non-doped hydride-terminated SiNPs (H-SiNPs; d < 70 nm)
108 prepared using a well-established procedure. The dimensions of the particles studied here are
109 approximately one to two orders of magnitude smaller than those previously reported and do not bear
110 any passivating amorphous "SiO_x" surface layer. We demonstrate that dangling bonds at the Si-H
111 terminated surface are present, although in very low concentrations, and that they enable modest

112 direct ^{29}Si DNP enhancements of the particles using high-field DNP NMR spectroscopy at 400 MHz
113 / 263 GHz and 600 MHz / 395 GHz, at sample temperatures of approximately 100 K.
114
115 **2. MATERIALS & METHODS**
116 H-SiNP Synthesis:
117 Hydride-terminated SiNPs were prepared using a well-established procedure as outlined by Hessel *et*
118 *al.* [44] and characterized via Fourier transform infrared spectroscopy, powder X-ray diffraction, X-
119 ray photoelectron spectroscopy and transmission electron microscopy, to verify purity and size
120 distribution as reported in Thiessen *et al.* [45].
121
122 Materials Characterization:
123 *Electron paramagnetic resonance spectroscopy of H-SiNPs:* EPR experiments were performed
124 directly on DNP samples using a 9.4 GHz X-band Bruker EMXnano spectrometer equipped with a 5
125 mm sample holder. DNP samples were packed in 3.2 mm sapphire rotors, which were directly
126 inserted into the 5 mm EPR tube and centered in the cavity using a guide. Continuous-wave X-band
127 EPR spectra were acquired with a center field of 3430 G, sweep width of 400 G, modulation
128 amplitude of 4.0 G, and sweep time of 60 s. Spectra were processed in the Bruker Xenon software
129 using a digital filter width of 10 pts. For radical concentration measurements by EPR, the SpinCount
130 module of the Xenon software was used: EPR spectra were baseline corrected using only a zero-order
131 (DC) correction, then double integrated for spin counting. Radical concentrations were calculated
132 accounting for cavity Q, experimental parameters, and sample dimensions.
133
134 *Dynamic nuclear polarization nuclear magnetic resonance spectroscopy of H-SiNPs:* DNP NMR
135 samples were packed under an inert atmosphere in 3.2 mm sapphire rotors with zirconia top caps; for

136 the exogenous radical samples, a silicone rubber plug was placed between the sample and the
137 zirconia top cap. Silicon-29 DNP NMR spectra were recorded using low-temperature 3.2 mm double
138 resonance (HX) and triple resonance (HXY) MAS DNP probes at 14.1 and 9.4 T, respectively,
139 doubly tuned to ^{1}H ($\boldsymbol{\nu}_{\mathrm{L}}$ = 600.301 MHz and 400.049 MHz) and ^{29}Si ($\boldsymbol{\nu}_{\mathrm{L}}$ = 119.262 MHz and 79.471
140 MHz). All DNP NMR data were acquired at temperatures between 95 and 104 K, with magic angle
141 spinning at a frequency of 8 kHz, 1.3 x T_B recycle delays and between 4 and 128 co-added transients.
142 Spectra were referenced with respect to the ^{13}C signals of DSS (40.48 ppm) [46]. The DNP field
143 profile was performed by sweeping the main magnetic field of the NMR magnet (equipped with a
144 sweep coil) between 9.374 and 9.398 T (399.1 and 400.1 MHz, ^{1}H nuclear Larmor frequency). The
145 NMR magnetic field position was adjusted to the maximum of the ^{1}H (nitroxide biradical) and ^{29}Si
146 (endogenous radical) DNP NMR enhancements determined from their respective field profiles. A
147 low-power klystron source (Communications and Power Industries (CPI), Georgetown, Canada [47,
148 48] was used to generate microwaves with a fixed frequency of 263.58 GHz and an output power of
149 5.6 W (>5 W at the sample), as verified using a PM5-VDI/Erickson Power Meter (Virginia Diodes
150 Inc., Charlottesville, VA).
151 <u>Indirect DNP NMR of an exogenous radical:</u> Indirect DNP NMR experiments were performed using
152 a 14.1 T (600 MHz, ^{1}H) Bruker Avance III HD DNP NMR spectrometer equipped with a 395 GHz
153 gyrotron microwave source delivering high-power microwaves (~16 W) to the sample. Cross-
154 polarization [1] (CP) ^{29}Si{^{1}H} DNP MAS NMR experiments were performed using a mixing time of
155 8.0 ms and an optimized Hartmann-Hahn match condition with a 20% tangential ramp on ^{1}H. The H-
156 SiNP samples were placed into sapphire rotors with the addition of 20 mM biradical / toluene
157 solution (90% toluene-d_8, 10% toluene) added, followed by slight agitation to ensure wetting of the
158 complete sample; the biradical used was either AMUPol or bCTbK. Toluene was used to suspend
159 hydride-terminated SiNPs and protect the particles from oxidizing as it demonstrates good glassing

ability [49] and is an appropriate solvent to dissolve hydrophobic (e.g. bCTbK) nitroxide-based radicals, as well more hydrophilic biradicals (e.g. AMUPol) at high-mM concentrations.

Direct DNP NMR of endogenous radical: Direct DNP NMR experiments were performed on a 9.4 T (400 MHz, ^{1}H) Bruker Avance III HD DNP NMR spectrometer with a 263 GHz EIK microwave source using either a flip-back Bloch [50, 51] or Hahn-echo [52] pulse sequence on ^{29}Si ($\boldsymbol{\gamma}B_1/2\pi$ = 71 kHz) using CW proton decoupling ($\boldsymbol{\gamma}B_1/2\pi$ = 71 kHz).

DNP buildup times: Silicon-29 nuclear buildup times were determined using a saturation recovery [53] experiment with 16 pre-saturation pulses (both ^{1}H and ^{29}Si) and two co-added transients per data point with varying relaxation delays from 1.0×10^{-3} to 600 s for the 3 nm H-SiNP and 3.0×10^{-5} to 2.8 hours for 6, 9, 21, and 64 nm H-SiNPs.

3. Results & Discussion

Hydride-terminated SiNPs prepared through the thermal disproportionation of hydrogen silsesquioxane (HSQ) demonstrate a core-shell type structure, as shown in Figure 1b [45]. The surface is comprised of a mixture of Si-H, Si-H_2 and Si-H_3 species which together lead to a disordered surface structure. In contrast, the nanoparticle core is typically comprised of well-ordered crystalline silicon (diameters > 6 nm). In between the inner and surface layers is a semi-ordered subsurface, which is comprised of a disordered array of silicon atoms that are more ordered than the surface, but less ordered than the crystalline core. The subsurface structure is attributed to the influence of the mismatch between the crystalline Si and the SiO_2-like matrix in which the nanoparticles nucleate and grow [54,55].

Following the proposed structure, it is reasonable that most of the unpaired electrons should be localized within the nanoparticle surface and subsurface layers, where there is less order and dangling bonds are more likely to be present. As outlined previously by Cassidy *et al.*, there should be very

184 few unpaired electrons in the crystalline core [56]. They suggested unpaired electrons lie at the
185 interface between the Si/SiO_2 passivating layer. Despite having a hydride-terminated surface, we
186 expect that a similar argument applies in the present system, suggesting the unpaired electrons are
187 located on (or in close proximity to) the surface of the particles. This proposal is further supported by
188 previous work showing that oxidation of the Si-H particles passivates surface defects, decreasing the
189 number of dangling bonds in the system as studied by EPR [57]. In this context, while we cannot
190 discount the presence of unpaired electrons in the nanoparticle core, their contribution will be
191 minimal relative to the concentration of unpaired electrons localized on the surface.

192 An alternative potential source of unpaired electrons in the SiNP core may come from nitrogen
193 incorporation, much as with nitrogen vacancies in diamond [58]. However, it is well established that
194 even trace nitrogen impurities in the SiNPs will result in a dramatic change in their
195 photoluminescence and manifest as a shift from characteristic red (or near-IR) to blue emission [59];
196 no such spectral change is observed for the materials investigated. Furthermore, nitrogen and other
197 impurities were not detected in the XPS and EDX analyses of our samples at the detection limit of
198 the methods.

199 Two DNP NMR protocols were examined here to determine the most effective approach to study
200 a series of hydride-terminated SiNPs. The first method employed nitroxide biradicals incorporated
201 into a glassing agent (e.g., glycerol/water, DMSO/water, TCE, toluene, etc.). This approach is
202 optimized for polarizing ^{1}Hs and indirectly enhancing the ^{29}Si nuclei through CP. The second
203 approach was to determine whether one can effectively enhance the silicon directly without adding
204 an exogenous radical; that is, to utilize the intrinsic endogenous radical present on the SiNPs as a
205 direct ^{29}Si polarizing agent.

206

207 Exogenous Organic Biradical using an Indirect DNP Transfer ($e^- \rightarrow {}^{1}H \rightarrow {}^{29}Si$)

208 Using the conventional approach, a 20 mM biradical solution was prepared in 90% toluene-d_8
209 and added to the H-SiNPs, protecting the surface of the particle from oxidation. It is well-established
210 that silicon particle surfaces readily react with radicals [60,61]; the latter were studied using EPR
211 spectroscopy at room temperature. In Table 1, we can identify the rapid change within the initial
212 radical concentration (20 mM) and subsequent slower radical quenching via time series
213 measurements. The 9.4 GHz EPR spectrum reveals radical decomposition occurring immediately,
214 with only a small fraction (i.e., 13 mM) of the original radical concentration remaining after a few
215 minutes at room temperature (i.e., the time required for the transfer from the glove box to the EPR).
216 In under 30 minutes, the radical concentration is nearly an order of magnitude lower and within one
217 day, there is no evidence of the biradical even when stored at cryogenic temperatures. The resulting
218 EPR signal that remains arises as a result of the dangling bonds on SiNPs, with no detectable signal
219 from a nitroxide containing mono- or biradical. Although this test was completed using 20 mM
220 AMUPol/90:10 toluene-d_8/toluene, similar effects were observed on the more structurally rigid
221 bCTbK biradical. To work within this short time can be challenging, but, as shown in Figure 1c, a
222 DNP-enhanced ^{29}Si{^{1}H} CP MAS NMR spectrum of 64 nm H-SiNP was obtained at 600 MHz / 395
223 GHz using bCTbK, achieving an enhancement of 3 for the broad resonance (-80 to -120 ppm). As
224 assigned in a previous study by Thiessen *et al.* [45], this broad resonance corresponds to Si-H_x
225 species on the NP surfaces. Since the polarization transfer goes from the unpaired electrons to ^{1}H to
226 ^{29}Si, it is not surprising that only the surface and some sub-surface regions of the SiNP show an
227 enhancement. After 12 hours at cryogenic temperatures, no further enhancement was observed; this
228 can be readily understood by considering the absence of nitroxide radical within the prepared sample
229 and later confirmed using X-band EPR spectroscopy.
230

Table 1: Total radical concentrations (endogenous and exogenous) measured using X-band EPR of 64 nm H-SiNP after quenching with 20 mM AMUPol in 90:10 toluene-d_8 / toluene.

Time after Quench	[Radical] (mM) (± 0.1)	e^- (mM)
DNP Solution	20	40
H-SiNP	0.6	0.6
1 min	13.1	25.6
30 min	3.9	7.3
1.5 days	0.6	0.6

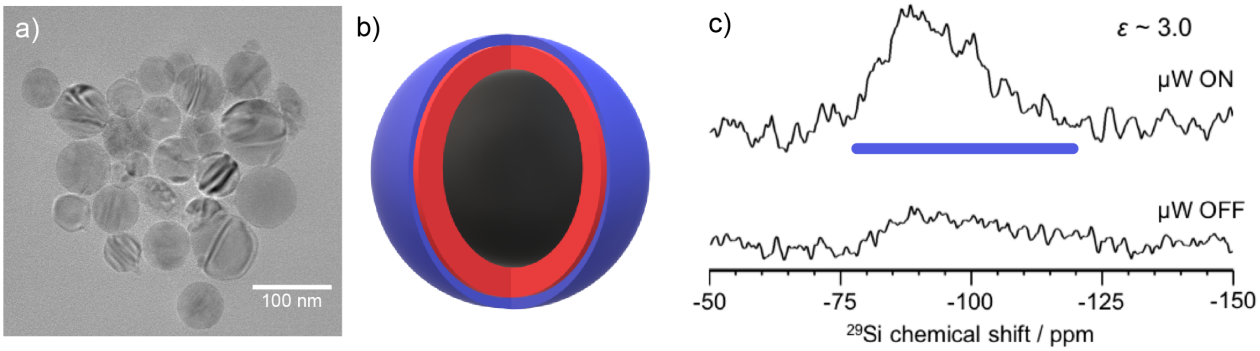

Figure 1: a) TEM image of the 64 nm H-SiNP, b) schematic of a particle identifying the three regions of a SiNP, namely core (black), sub-surface (red) and surface (blue) and c) DNP-enhanced (μW on) and non-DNP-enhanced (μW off) ^{29}Si{^{1}H} CPMAS NMR spectra of 64 nm hydride-terminated SiNP using 20 mM bCTbk in 90:10 toluene-d_8 / toluene. The spectrum in (c) was recorded within 15 minutes of the addition of exogenous radical. Typically, during the course of these experiments, glove-box sample preparation and rotor insertion into a DNP probe would require ~ 3-5 minutes; establishing stable spinning and reaching a set point temperature would take another approximately 3-5 minutes.

As a result of the reactive dangling bonds as well as the hydride-terminated SiNP surfaces, the exogenous biradicals are effectively deactivated. The influence of dangling bonds has been demonstrated in studies where the monoradical TEMPO reacts with Si dangling bonds and becomes

coordinated to the Si surface [60,61]. Of particular concern in this study is the complete elimination of both radicals from the added biradical / toluene solution after only one day. Based upon what has been reported as a radical coupling reaction between the Si (nanoparticle) and O (biradical) atoms, in principle one would expect the secondary O radical present should still be detected after the initial radical coupling reaction and thus should contribute to the overall radical concentration (i.e., forming a monoradical attached to the nanoparticle surface). However, as shown in Table 1, the net organic radical concentration after 1.5 days is ~ 0, suggesting that both radicals on the organic polarizing agent have been deactivated. Although, the mechanism in which this occurs is not presently known, radical reactions on hydride-terminated silicon surface are known (*e.g.,* radical-initiated hydrosilylation) [61]. A possible explanation is that the biradical is quenched via a mechanism similar to radical initiated hydrosilylation, where the NO radical abstracts an H·(dot) from the surface to form HNO; leaving a Si·(dot) on the surface stabilized by the particle. This Si·(dot) can further react with another NO radical, quenching the biradical species, while leaving the dangling bond on SiNPs active. Further insight into the reaction between the NO radical and the H-SiNP is the subject of ongoing investigations.

Endogenous Radical using Direct DNP Transfer

Shifting to smaller particles at higher magnetic fields and temperatures creates a variety of challenges. In earlier microparticle work, Dementyev *et al*. and Aptekar *et al.* showed a decrease in T_1 with decreasing particle size [39,62]. As T_1 decreases, less time is available to effectively allow ^{29}Si-^{29}Si spin-diffusion across the sample, leading to a reduction in the ability to build up polarization (i.e., lower enhancements). While going to higher magnetic fields (9.4 /14.1 vs. 2.35 T) increases the nuclear spin-lattice relation time for ^{1}H and ^{29}Si, both the CE and SE polarization mechanisms scale inversely (i.e., ~ $1/B_0$ and $1/B_0^2$, respectively) with magnetic field strength, which can impact the

271 DNP NMR enhancements. One also needs to consider the number of dangling bonds due to the onset
272 of paramagnetic relaxation and signal quenching. This will have a greater impact on smaller particles
273 (d < 10 nm) where the surface comprises a significant portion of the solid, impacting both spin-lattice
274 relaxation times and NMR lineshapes [45], as well as effective electron-nuclear polarization transfer.

275 To assess the feasibility of these pristine H-SiNPs for direct ^{29}Si DNP NMR at high fields, a
276 range of particle sizes were characterized using EPR measurements to determine the radical
277 concentration present on/in the surface/subsurface of the nanoparticles. Table 2 shows the range of
278 radical concentrations associated with SiNPs studied here; in all cases (i.e., d~3 to 64 nm)
279 concentrations are less than 1 mM, consistent with the unpaired electrons arising from dangling
280 bonds residing on the surface layers. The chemical treatment or doping of these particles is a
281 promising avenue worth exploring in efforts to assess the impact surface modification may play in
282 achieving further gains in DNP enhancements.

283

284 **Table 2: Endogenous radical concentrations, enhancement factors (ε), and buildup times (T_B)**
285 **for a series of H-SiNPs.**

Particle diameter (TEM) /nm	Annealing Temperature / °C	Radical Concentration /mM	Enhancement (ε)	Buildup Time (T_B) [c] /s
3	1100	0.69	1.5	193
6	1200	0.16 / 0.10[a]	0.92 - 0.94[b]	270
9	1300	0.47 / 0.10[a]	1.0	1733
21	1400	0.22	1.23	3961
64	1500	0.70 / 0.42[a]	1.5 - 6.0[b]	4733

a. Two batches of H-SiNPs were synthesized to compare endogenous radical concentrations
b. Ranges correspond to different H-SiNP batches studied, as well as variations in surface/sub-surface vs. core enhancements (0.7 mM is responsible for ε of 6)
c. Buildup times for larger particles (21 and 64 nm) are underestimated due to experimental time constraints to fully extrapolate the long T_B values.

286

287 Figure 2 shows a partial field profile obtained for H-SiNPs of average diameter 64 nm (TEM) that
288 reveals the maximum positive and negative enhancement regions at 9.4 T. Under the conditions
289 investigated here with higher magnetic field strengths and cryogenic liquid nitrogen temperatures,
290 two dominant mechanisms can be considered to effectively enable electron–nuclear polarization
291 transfer: cross-effect (CE) and solid-effect (SE). Although both mechanisms can occur, each has a
292 different set of criteria that must be satisfied if DNP enhancement is to occur. Broadly, the CE
293 mechanism involves a three-spin process involving two electrons and a nuclear spin that are dipolar
294 coupled, whereby the difference in the Larmor frequencies ($\omega_{0S1,2}$) of the two electron spins should
295 approximate the nuclear Larmor frequency (ω_{0I}), where $\omega_{0I} = | \omega_{0Si} - \omega_{0Sii}|$. CE is the dominant
296 mechanism for exogenous nitroxide-containing mono- and biradicals, as their inhomogeneous
297 linewidth of their EPR spectrum is larger than the nuclear Larmor frequency (i.e., 9.4 T – 400 MHz
298 (^{1}H) or 79.5 MHz (^{29}Si)), while the homogeneous component is smaller. Conversely, the two-spin SE
299 mechanism can occur when microwave irradiation is applied at the electron-nuclear zero- or double-
300 quantum frequency, where $\omega_{\mu w} = \omega_{0I} \pm \omega_{0S}$. The SE mechanism is typically dominant when the EPR
301 spectrum is narrow (i.e., when inhomogeneous and homogeneous linewidths are less than the nuclear
302 Larmor frequency) [7, 30, 32, 33, 63-67].

303 The appearance of the EPR resonance and measured field profile (Figure 2a) exhibits a full-
304 width-at-half-maximum of ~45 MHz and a full-width-at-the-base of ~96 MHz. The narrow EPR
305 lineshape of 45 MHz (which is less than the ^{29}Si nuclear Larmor frequency of 79.5 MHz), low radical
306 concentration (< 1 mM, low probability of e^- --- e^- dipole coupling), and nearly symmetric positions
307 of the positive and negative maxima, would appear to be consistent with a SE DNP mechanism.
308 However, some finer features appear to be lacking, bringing into question whether a contribution
309 from cross-effect can be completely excluded. For example, no plateau is noted between the positive
310 and negative maxima of the symmetric featureless field profile, as is often the case for CE but not

SE. The separation between positive and negative enhancement is larger than the expected, $2\omega_{oI}$ = 159 MHz, and the EPR spectrum, at its base, is larger than the ^{29}Si nuclear Larmor frequency (96 MHz > 79.5 MHz). Lastly, the enhancement does not appear to increase with microwave power (i.e., appears saturated) at only ~5 W of output power; while this is not uncommon for the CE, SE typically requires significantly more power to saturate. Therefore, further studies are needed to assess the dominant DNP mechanism between solid- and cross-effect including higher endogenous radical concentration and higher microwave power (i.e., gyrotron vs. klystron). Increasing the ^{29}Si enhancement and multiple field studies may provide assessment and refinement of the finer nuances within the DNP field profile to determine which mechanism is dominant; studies are ongoing. We note that the overall field profile resembles that observed in a ^{29}Si DNP NMR study of microparticles that were recorded at lower temperatures and magnetic fields and contained higher radical concentrations; in this case the authors attributed the behavior to a thermal mixing process [39].

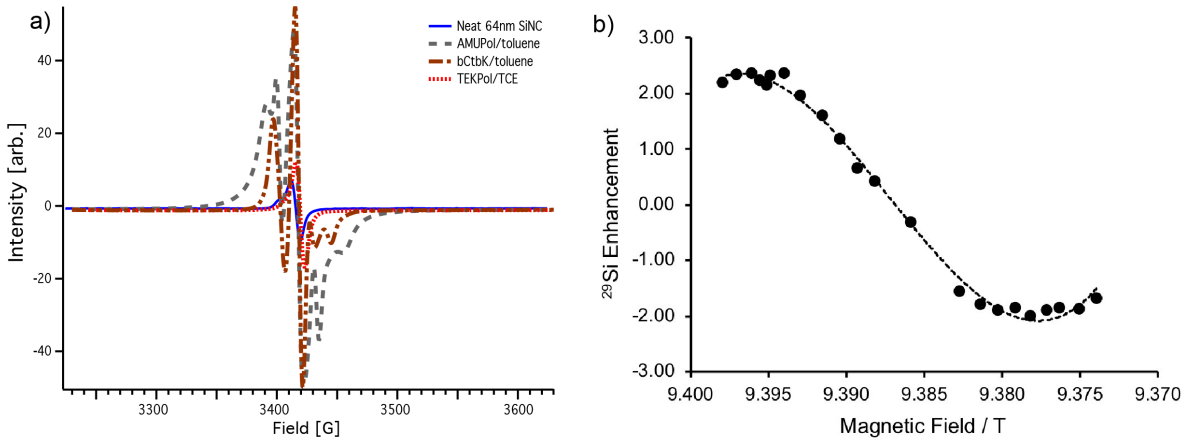

Figure 2: a) X-band EPR spectra of 64 nm H-SiNP and indicated nitroxide biradicals and b) particle field-profile for ^{29}Si direct DNP of 64 nm hydride-terminated SiNPs at 95 K with MAS frequency of 8 kHz.

329 Table 2 summarizes the enhancements observed for the series of H-SiNPs investigated here. The
330 ^{29}Si DNP NMR spectrum for the 64 nm H-SiNP is shown in Figure 3, along with an NMR
331 (microwave off) spectrum. An enhancement of 6 was obtained for the sharp resonance at $\delta_{iso} \approx$ -85
332 ppm at 100 K ($\delta_{iso} \approx$ -81 ppm at 300 K) corresponding to the highly ordered (diamond lattice)
333 crystalline SiNP core [45]. The observed change in the ^{29}Si chemical shift of the core is consistent
334 with our previous study of the interplay between the band gap and ^{29}Si chemical shift, as the 64 nm
335 particles band gap increases to 1.16 eV at 100 K vs. 1.12 eV at 300 K [68, 69]. Furthermore, a low
336 intensity resonance that is sharper than the surface ^{29}Si shown in Figure 1 but broader than the sharp
337 core resonance is observed at lower frequency ($\delta_{iso} \approx$ -93 ppm) and attributed to the intermittent
338 subsurface layer [45]. Although the enhancement is quite small, it was obtained from an endogenous
339 radical concentration of 0.70 mM. We believe that if this radical concentration could be increased by
340 an order of magnitude, the samples would more easily satisfy the three-spin condition for CE, leading
341 to increased DNP enhancements. Nevertheless, the current enhancement, providing a 36-fold
342 reduction in experimental time, demonstrates the practicality of studying SiNP via direct ^{29}Si DNP
343 from the dangling bonds residing near the surface of the H-SiNPs. Unfortunately, marginal
344 enhancements were obtained for particles smaller than 64 nm. This may arise from lower
345 concentrations of endogenous radicals (< 0.5 mM for 6, 9, and 21 nm H-SiNPs), as well as shorter
346 polarization buildup times (0.05 h for 3 nm vs. > 1.3 h for 64 nm H-SiNPs) mitigating effective ^{29}Si
347 spin diffusion. The primary interactions responsible for the relaxation behavior of these rigid
348 materials are a balance between ^{29}Si-^{29}Si homonuclear dipolar coupling and paramagnetic relaxation,
349 whereby the smaller particles with larger surface areas are more greatly impacted by the unpaired
350 electrons from dangling bonds. As the particle increases in size, further ordering in the diamond-

351 lattice crystalline core causes the dangling bonds to be isolated on the surface, thereby increasing
352 overall ^{29}Si spin-lattice relaxation.
353

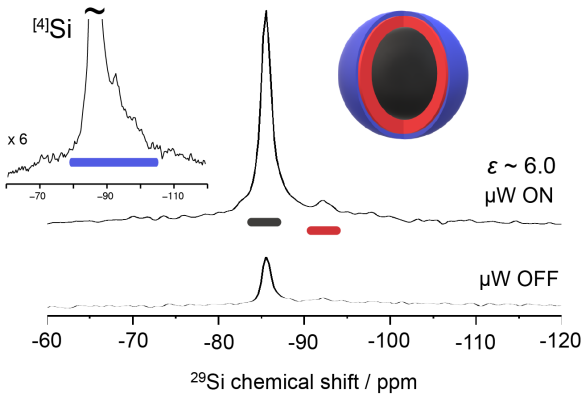

354

355 **Figure 3: Silicon-29 DNP NMR spectrum of hydride-terminated SiNPs (64 nm) with an**
356 **endogenous radical acquired at a MAS frequency of 8 kHz (μW on). The corresponding**
357 **spectrum acquired without microwave irradiation (μW off). Inset is the μW on spectrum**
358 **vertically scaled by 6 to illustrate the surface (blue) of the H-SiNP. The ^{29}Si resonance at -85**
359 **ppm is signal from the crystalline core and the small shoulder to lower frequency (red) is**
360 **subsurface [45].**
361
362 As the DNP process requires the ability to transfer electron polarization (radical source) to its
363 surrounding nuclear environment, the subsequent process of nuclear – nuclear spin diffusion is also a
364 vital component, in particular when dealing with inhomogeneous radical distributions; this is often
365 the case when dealing with crystalline solids. Recently, Wittman *et al.* described a detailed study
366 looking at endohedral fullerene, N@C_{60} sparsely diluted in C_{60} to understand the spin-diffusion
367 barrier under MAS DNP conditions [70]. Thus, they determined electron driven spin-diffusion
368 strongly polarizes the nuclei near the radical (< 15 Å), however, this region of the sample does not
369 contribute to the NMR signal due to impacts on the chemical shifts (paramagnetic interaction) and
370 rapid relaxation. The nuclei near the radical polarizes more efficiently at slower spinning frequencies

371 (~ 10 Å) while faster MAS improves the polarization transfer of nuclei further away (> 15 Å). This
372 services as evidence of a long-hypothesized spin diffusion barrier [28, 70, 71] over which
373 polarization must somehow cross in order to achieve long-range diffusion and thereby achieve
374 overall polarization of the sample nuclei. Another important point they discussed through spin-
375 diffusion simulation work is that direct DNP without relay transfer through the nuclear spin network
376 (i.e., inhibiting homonuclear spin diffusion) resulted in no bulk enhancement, as one would expect.
377 Therefore, an efficient crossing of the diffusion barrier will lead to the ability in obtaining a larger
378 polarization of the bulk material, although, if the spin diffusion is hampered by a low concentration
379 of NMR active nuclear spins (e.g., ^{13}C or ^{29}Si as in our case), this will cause a slower build-up in
380 DNP polarization. In the same year, Björgvinsdóttir *et al.* discussed an expression for non-spinning
381 samples whereby high polarization of micrometer-sized solids may be achieved through homonuclear
382 spin-diffusion between low-ɣ nuclei [72]. As they pointed out, homonuclear spin diffusion is often
383 neglected for low-ɣ nuclei due to weak dipolar interaction (e.g., ^{29}Si-^{29}Si in SiNPs is 366 Hz,
384 diamond structure, Fd-3m space group). Therefore, even under moderate spinning frequencies one
385 can remove these weak couplings and mitigate spin diffusion [73]. However, only at infinite spinning
386 frequency does the diffusion coefficient go to zero, while under MAS the authors note that one can
387 estimate a decrease of an order or two in magnitude.

388 How this may impact our results is difficult to directly assess due to the range of endogenous
389 radicals (~100 to 700 ppm), distribution in the sizes of the particles (e.g., 3 ± 1 vs. 64 ± 18 nm) and
390 definitive knowledge of the dangling bond locations (i.e. surface/subsurface region). Nonetheless, the
391 three smallest SiNPs (3, 6 and 9 nm) satisfy the regime where the dangling bonds will influence a
392 large portion of the ^{29}Si nuclear spins with particle radii of 15 ± 5 Å, 30 ± 5 Å and 45 ± 5 Å;
393 considering paramagnetic centers will have direct spherical influence up to ~25 Å [70, 74] and the
394 surface/subsurface layers will comprise ~ the first 10 Å. Therefore, we can hypothesize an effective

electron-nuclear polarization relay to dominate with a minor nuclear spin-diffusion role. As predicted by Wittman *et al.*, the resulting polarization enhancement for these small particles using direct ^{29}Si DNP is poor [70]. These smaller particles may be best enhanced via indirect DNP through the introduction of exogenous organic radicals if one could circumvent their highly reactive surfaces. The larger 64 nm particle (r = 320 Å) however, demonstrates a long build-up time with a reasonable DNP enhancement of 6 of the sharp resonance assigned to the core, the minor resonance to lower frequency from the sub-surface, and the broader component nearly hidden for the surface, vide supra. Therefore, with the radicals isolated to the surface/sub-surface, the region likely to directly receive polarization from unpaired electrons is within 30 to 40 Å of the surface. Transiting the last ~280 Å towards the core would require some type of ^{29}Si-^{29}Si homonuclear spin-diffusion; based on the long build-up times observed for these materials, the latter process must be fairly efficient in these samples, with minimal relaxation. Although the spin diffusion will be small and slow (4.7 % natural abundance, low-γ), the long relaxation times assist in relaying this polarization inward. Using the approach described by Björgvinsdóttir *et al.* [72], the estimated ^{29}Si spin diffusion coefficient for SiNPs is 12 nm^2/s (i.e., non-spinning conditions). If we assume MAS will decrease the diffusion coefficient by 10^2, a potential bulk polarization gain of 90 is calculated. In sum, our results are consistent with those of the aforementioned reports on model systems, however, further studies are essential to untangle the complex contributions related to the DNP mechanism, radical location and radical concentration in SiNPs.

4. Conclusion

In this work, we discuss two DNP NMR protocols to study a series of H-SiNPs. Using EPR, it was observed that, with the conventional DNP NMR approach, the exogenous biradical concentration was reduced significantly within minutes, hampering effectiveness in bulk materials. Thus, the reactive

419 nature of the hydride surfaces renders the use of exogenous radicals for indirect DNP transfer
420 impractical for the study of H-SiNPs. Building upon DNP studies on silicon microparticles using
421 direct ^{29}Si DNP from intrinsic dangling bonds on the Si surface/sub-surface, we demonstrated the
422 ability to obtain good ^{29}Si DNP enhancements ($\varepsilon = 6$ for 64 nm H-SiNPs) from the low endogenous
423 radical concentrations of < 1 mM at high magnetic fields. These promising preliminary results
424 demonstrate the potential for direct DNP polarization transfer using endogenous radicals, followed by
425 ^{29}Si homonuclear spin-diffusion into the core of the particle assisted by long spin-lattice relaxation
426 values. Future developments in surface modification to control dangling bond formation as well as
427 size control may lead to further gains in sensitivity and the interplay between radical-nuclear
428 polarization transfer and low-γ homonuclear spin diffusion.

429

430 **ACKNOWLEDGEMENTS**

431 The Natural Sciences and Engineering Research Council (NSERC) of Canada Discovery Program
432 (RGPIN-2015-03896 and 2016-05547), NSERC CREATE supported Alberta/Technical University of
433 Munich International Graduate School for Hybrid Functional Materials (ATUMS, CREATE-463990-
434 2015), Future Energy Systems (CFREF Program at the University of Alberta Projects T06-Z01 and
435 T12-Z01) and the University of Alberta are acknowledged for their generous research support. M.H.
436 is partially supported by the Government of Alberta Queen Elizabeth II Scholarship. A.N.T. is
437 supported by the Alberta Innovates Graduate Student Scholarship and the Government of Alberta
438 Queen Elizabeth II Graduate Scholarship. DNP spectrometer time was kindly provided by Bruker
439 Biospin at their Billerica, MA (USA) facility.

REFERENCES

[1] A. Pines, M.G. Gibby, J.S. Waugh, Proton-Enhanced Nuclear Induction Spectroscopy. A Method for High Resolution NMR of Dilute Spins in Solids, J. Chem. Phys. 56 (1972) 1776-1777. https://doi.org/10.1063/1.1677439.

[2] E.R. Andrew, A. Bradeuey, R.G. Eades, Nuclear Magnetic Resonance Spectra from a Crystal Rotated at High Speed, Nature 182 (1958) 1659. https://doi.org/10.1038/1821659a0.

[3] I.J. Lowe, Free Induction Decays of Rotating Solids, Phys. Rev. Lett. 2 (1959) 284-287. https://doi.org/10.1103/PhysRevLett.2.285.

[4] E.G. Keeler, V.K. Michaelis, M.T. Colvin, I. Hung, P.L. Gor'kov, T.A. Cross, Z. Gan, R.G. Griffin, ^{17}O MAS NMR Correlation Spectroscopy at High Magnetic Fields, J. Am. Chem. Soc. 139 (2017) 17953-17963. https://doi.org/10.1021/jacs.7b08989.

[5] A.W. Overhauser, Polarization of Nuclei in Metals, Phys. Rev. 92 (1953) 411-415. https://doi.org/10.1103/PhysRev.92.411.

[6] T.R. Carver, C.P. Slichter, Polarization of Nuclear Spins in Metals, Phys. Rev. 92 (1953) 212-213. https://doi.org/10.1103/PhysRev.92.212.2.

[7] T. Maly, G.T. Debelouchina, V.S. Bajaj, K. Hu, C. Joo, M.L. Mak-Jurkauskas, J.R. Sirigiri, P.C.A. van der Wel, J. Herzfeld, R.J. Temkin, R.G. Griffin, Dynamic nuclear polarization at high magnetic fields, J. Chem. Phys. 128 (2008) 052211. https://doi.org/10.1063/1.2833582.

[8] M. Ha, V.K. Michaelis, High-Frequency Dynamic Nuclear Polarization NMR for Solids: Part 2 – Development and Applications, in: G.A. Webb (Ed.), Modern Magnetic Resonance 2nd ed., Springer International Publishing AG, 2017, pp. 1-18. https://doi.org/10.1007/978-3-319-28275-6_141-1.

[9] C. Song, K-N. Hu, C-G. Joo, T.M. Swager, R.G. Griffin, TOTAPOL: A Biradical Polarizing Agent for Dynamic Nuclear Polarization Experiments in Aqueous Media, J. Am. Chem. Soc. 128 (2006) 11385-11390. https://doi.org/10.1021/ja061284b.

[10] M.K. Kiesewetter, B. Corzilius, A.A. Smith, R.G. Griffin, T. M. Swager, Dynamic Nuclear Polarization with a Water-soluble Rigid Biradical, J. Am. Chem. Soc. 134 (2012) 4537-4540. https://doi.org/10.1021/ja212054e.

[11] C. Sauvée, M. Rosay, G. Casano, F. Aussenac, R.T. Weber, O. Ouari, P. Tordo, Highly efficient, water-soluble polarizing agents for dynamic nuclear polarization at high frequency. Angew. Chem. Int. Ed. 52 (2013), 10858-10861. https://doi.org/10.1002/anie.201304657.

[12] A. Zagdoun, G. Casano, O. Ouari, M. Schwarzwälder, A.J. Rossini, F. Aussenac, M. Yulikov, G. Jeschke, C. Copéret, A. Lesage, P. Tordo, L. Emsely, Large molecular weight nitroxide biradicals providing efficient dynamic nuclear polarization at temperatures up to 200 K, J. Am. Chem. Soc. 135 (2013) 12790-12797. https://doi.org/10.1021/ja405813t.
[13] D. J. Kubicki, G. Casano, M. Schwarzwälder, S. Abel, C. Sauvée, K. Ganesan, M. Yulikov., A.J. Rossini, G. Jeschke, C. Copéret, A. Lesage, P. Tordo, O. Ouari, L. Emsley, Rational design of dinitroxide biradicals for efficient cross-effect dynamic nuclear polarization, Chem. Sci. 7 (2016) 550-558. https://doi.org/10.1039/C5SC02921J.
[14] T.C. Ong, M.L. Mak-Jurkauskas, J.J. Walish, V.K. Michaelis, B. Corzilius, A.A. Smith, A.M. Clausen, J.C. Cheetham, T.M. Swager, R.G. Griffin, Solvent-Free Dynamic Nuclear Polarization of Amorphous and Crystalline *ortho*-Terphenyl, J. Phys. Chem. B 117 (2013) 3040-3046. https://doi.org/10.1021/jp311237d.
[15] C. Sauvée, G. Casano, S. Abel, A. Rockenbauer, D. Akhmetzyanov, H. Karoui, D. Siri, F. Aussenac, W. Maas, R.T. Weber, T. Prisner, M. Rosay, P. Tordo, O. Ouari, Tailoring of polarizing agents in the bTurea series for cross-effect dynamic nuclear polarization in aqueous media. Chem. Eur. J. 22 (2016) 5598-5606. https://doi.org/10.1002/chem.201504693.
[16] Y. Matsuki, T. Maly, O. Ouari, H. Karoui, F. Le Moigne, E. Rizzato, S. Lyubenova, J. Herzfeld, T. Prisner, P. Tordo, R.G. Griffin, Dynamic nuclear polarization with a rigid biradical, Angew. Chem. Int. Ed. 48 (2009) 4996-5000. https://doi.org/10.1002/anie.200805940.
[17] A. Zagdoun, G. Casano, O. Ouari, G. Lapadula, A.J. Rossini, M. Lelli, M. Baffert, D. Gajan, L. Veyre, W.E. Maas, M. Rosay, R.T. Weber, C. Thieuleux, C. Coperet, A. Lesage, P. Tordo, L. Emsley, A Slowly Relaxing Rigid Biradical for Efficient Dynamic Nuclear Polarization Surface-Enhanced NMR Spectroscopy: Expeditious Characterization of Functional Group Manipulation in Hybrid Materials, J. Am. Chem. Soc. 134 (2012) 2284-2291. https://doi.org/10.1021/ja210177v.
[18] G. Mathies, M.A. Caproini, V.K. Michaelis, Y. Liu, K-.N., Hu, D. Mance, J.L. Zweier, M. Rosay, M. Bladus, R.G. Griffin, Efficient dynamic nuclear polarization at 800 MHz/527 GHz with trityl-nitroxide biradicals, Angew. Chem. Int. Ed. 54 (2015) 11770-11774. https://doi.org/10.1002/anie.201504292.
[19] F. Mentink-Bigier, G. Mathies, Y. Liu, A-L. Barra, M.A. Caporini, D. Lee, S. Hediger, R.G. Griffin, G. De Paëpe, Efficient cross-effect dynamic nuclear polarization without depolarization in high-resolution MAS NMR, Chem. Sci. 8 (2017) 8150-8163. https://doi.org/10.1039/C7SC02199B.

[20] D. Lee, S. Hediger, G. De Paëpe, High-Field Solid-State NMR with Dynamic Nuclear Polarization, in: G.A. Webb (Ed.), Modern Magnetic Resonance, Springer Cham, 2017, pp. 1-17. https://doi.org/10.1007/978-3-319-28275-6_73-1.
[21] Q.Z. Ni, E. Daviso, T.V. Can, E. Markhasin, S.K. Jawla, T.M. Swager, R.J. Temkin, J. Herzfeld, R.G. Griffin, High Frequency Dynamic Nuclear Polarization, Acc. Chem. Res. 46 (2013) 1933-1941. https://doi.org/10.1021/ar300348n.
[22] A.J. Rossini, A. Zagdoun, M. Lelli, A. Lesage, C. Copéret, L. Emsley, Dynamic Nuclear Polarization Surface Enhanced NMR Spectroscopy, Acc. Chem. Res. 46 (2013) 1942-1951. https://doi.org/10.1021/ar300322x.
[23] T. Maly, L.B. Andreas, A.A. Smith, R.G. Griffin, ^{2}H-DNP-enhanced ^{2}H-^{13}C solid-state NMR correlation spectroscopy, Phys. Chem. Chem. Phys. 12 (2012) 5872-5878. https://doi.org/10.1039/C003705B.
[24] V.K. Michaelis, B. Corzilius, A.A. Smith, R.G. Griffin, Dynamic Nuclear Polarization of ^{17}O: Direct Polarization, J. Phys. Chem. B 117 (2013) 14894-14906. https://doi.org/10.1021/jp408440z.
[25] V.K Michaelis, A.A. Smith, B. Corzilius, O. Haze, T.M Swager, R.G. Griffin, High-Field ^{13}C Dynamic Nuclear Polarization with a Radical Mixture, J. Am. Chem. Soc. 135 (2013) 2935-2938. https://doi.org/10.1021/ja312265x.
[26] V.K. Michaelis, T.C. Ong, M.K. Kiesewetter, D.K. Frantz, J.J. Walish, E. Ravera, C. Luchinat, T.M. Swager, R.G. Griffin, Topical Development in High-Field Dynamic Nuclear Polarization, Isr. J. Chem. 54 (2014) 207-221. https://doi.org/10.1002/ijch.201300126.
[27] B. Corzilius, A.A. Smith, R.G. Griffin, Solid effect in magic angle spinning dynamic nuclear polarization, J. Chem. Phys. 137 (2012) 054201. https://doi.org/10.1063/1.4738761.
[28] A.A. Smith, B. Corzilius, A.B. Barnes, T. Maly, R.G. Griffin, Solid effect dynamic nuclear polarization and polarization pathways, J. Chem. Phys. 136 (2012) 015101. https//doi.org/10.1063/1.3670019.
[29] A. Abragam, W.G. Proctor, Une Nouvelle Methode De Polarisation Dynamique Des Noyaux Atomiques Dans Les Solides, Cr. Hebd. Acad. Sci. 246 (1958), 2253-2256.
[30] C.F. Hwang, D.A. Hill, New Effect in Dynamic Polarization, Phys. Rev. Lett. 18 (1967) 110-112. https://doi.org/10.1103/PhysRevLett.18.110.

[31] Y. Hovav, A. Feintuch, S. Vega, Theoretical aspects of Dynamic Nuclear Polarization in the solid state – the cross effect, J. Magn. Reson. 214 (2012) 29-41. https://doi.org/10.1016/j.jmr.2011.09.047.
[32] M. Ha, V.K. Michaelis, High-Frequency Dynamic Nuclear Polarization NMR for Solids: Part 1 – An Introduction, in: G.A. Webb (Ed.), Modern Magnetic Resonance 2nd ed., Springer International Publishing AG, 2017, pp. 1-24. https://doi.org/10.1007/978-3-319-28275-6_140-1.
[33] K-N. Hu, V. Bajaj, M. Rosay, R.G. Griffin, High-frequency dynamic nuclear polarization using mixtures of TEMPO and trityl radicals, J. Chem. Phys. 126 (2007) 015101. https://doi.org/10.1063/1.2429658.
[34] W.R. Gunther, V.K. Michaelis, M.A. Caporini, R.G. Griffin, Y. Román-Leshkov, Dynamic Nuclear Polarization NMR Enables the Analysis of Sn-Beta Zeolite Prepared with Natural Abundance ^{119}Sn Precursors, J. Am. Chem. Soc. 136 (2014) 6219-6222. https://doi.org/10.1021/ja502113d.
[35] P. Wenk, M. Kaushik, D. Richter, M. Vogel, B. Suess, B. Corzilius, Dynamic nuclear polarization of nucleic acid with endogenously bound manganese, J. Biomol. NMR 63 (2015) 97-109. https://doi.org/10.1007/s10858-015-9972-1.
[36] T. Wolf, S. Kumar, H. Singh, T. Chakrabarty, F. Aussenac, A.I. Frenkel, D.T. Major, M. Leskes, Endogenous Dynamic Nuclear Polarization for Natural Abundance ^{17}O and Lithium NMR in the Bulk of Inorganic Solids, J. Am. Chem. Soc. 141 (2019) 451-462. https://doi.org/10.1021/jacs.8b11015.
[37] B. Corzilius, V.K. Michaelis, S.A. Penzel, E. Ravera, A.A. Smith, C. Luchinat, R.G. Griffin, Dynamic Nuclear Polarization of ^{1}H, ^{13}C, and ^{59}Co in a Tris(ethylenediamine)cobalt(III) Crystalline Lattice Doped with Cr(III), J. Am. Chem. Soc. 136 (2014) 11716-11727. https://doi.org/10.1021/ja5044374.
[38] R.T. Schumacher, C.P. Slichter, Electron Spin Paramagnetism of Lithium and Sodium, Phys. Rev. 101 (1956) 58-65. https://doi.org/10.1103/PhysRev.101.58.
[39] A.E. Dementyev, D.G. Cory, C. Ramanathan, Dynamic Nuclear Polarization in Silicon Microparticles, Phys. Rev. Lett. 100 (2008) 127601. https://doi.org/10.1103/PhysRevLett.100.127601.

[40] M.L. Guy, K.J. van Schooten, L. Zhu, C. Ramanathan, Chemisorption of Water on the Surface of Silicon Microparticles Measured by Dynamic Nuclear Polarization Enhanced NMR, J. Phys. Chem. C 121 (2017) 2748-2754. https://doi.org/10.1021/acs.jpcc.6b11065.
[41] M.H. Brodsky, R.S. Title, Electron Spin Resonance in Amorphous Silicon, Germanium, and Silicon Carbide, Phys. Rev. Lett. 23 (1969) 581-585. https://doi.org/10.1103/PhysRevLett.23.581.
[42] J.G.C. Veinot, Synthesis, surface functionalization, and properties of freestanding silicon nanocrystals, Chem. Comm. 40 (2006) 4160-4168. https://doi.org/10.1039/B607476F.
[43] H.A. Santos, E. Mäkilä, A.J. Airaksinen, L.M. Bimbo, J. Hirvonen, Porous silicon nanoparticles for nanomedicine: preparation and biomedical applications, Nanomedicine 9 (2014) 535-554. https://doi.org/10.2217/nnm.13.223.
[44] C.M. Hessel, E.J. Henderson, J.G.C. Veinot, Hydrogen Silsesquioxane: A Molecular Precursor for Nanocrystalline Si-SiO_2 Composites and Freestanding Hydride-Surface-Terminated Silicon Nanoparticles, Chem. Mater. 18 (2006) 6139-6146. https://doi.org/10.1021/cm0602803.
[45] A.N. Thiessen, M. Ha, R.W. Hooper, H. Yu, A.O. Oliynk, J.G.C. Veinot, V.K. Michaelis, Chem. Mater. 31 (2019) 678-688. https://doi.org/10.1021/acs.chemmater.8b03074.
[46] C.R. Morcombe, K.W. Zilm, Chemical shift referencing in MAS solid state NMR, J. Magn. Reson. 162 (2003) 479-486. https://doi.org/10.1016/S1090-7807(03)00082-X.
[47] M. Rosay, I. V. Sergeyev, L. Tometich, C. Hickey, A. Roitman, D. Yake, D. Berry, Opportunities and Challenges for EIK's in DNP NMR Applications, in: Int. Conf. Infrared, Millimeter, Terahertz Waves, IRMMW-THz, 2018. https://doi.org/10.1109/IRMMW-THz.2018.8510328.
[48] A. Roitman, M. Hyttinen, H. Deng, D. Berry, R. Machattie, Progress in power enhancement of sub-millimeter compact EIKs, in: Int. Conf. Infrared, Millimeter, Terahertz Waves, IRMMW-THz, 2017. https://doi.org/10.1109/IRMMW-THz.2017.8067093.
[49] B. Meyer, Low Temperature Spectroscopy, American Elsevier, New York, 1971.
[50] F. Bloch, Nuclear Induction, Phys. Rev. 70 (1946) 460-474. https://doi.org/10.1103/PhysRev.70.460.
[51] S. Björgvinsdóttir, B.J. Walder, A.C. Pinon, J.R. Yarava, L. Emsley, DNP enhanced NMR with flip-back recovery, J. Magn. Reson. 288 (2018) 69-75. https://doi.org/10.1016/j.jmr.2018.01.017.
[52] E.L. Hahn, Spin Echoes, Phys. Rev. 80 (1950) 580-594. https://doi.org/10.1103/PhysRev.80.580.

[53] R. Freeman, H.D.W. Hill, Fourier Transform Study of NMR Spin-Lattice Relaxation by "Progressive Saturation", J. Chem. Phys. 54 (1971) 3367-3377. https://doi.org/10.1063/1.1675352.
[54] B.G. Lee, D. Hiller, J.W. Luo, O.E. Semonin, M.C. Beard, M. Zacharias, P. Stradins, Strained Interface Defects in Silicon Nanocrystals, Adv. Funct. Mater. 22 (2012) 3223-3232. https://doi.org/10.1002/adfm.201200572.
[55] K. Kleovoulou, P.C. Kelires, Stess state of embedded Si nanocrystals, Phys. Rev. B 88 (2013) 085424. https://doi.org/10.1103/PhysRevB.88.085424.
[56] M.C. Cassidy, H.R. Chan. B.D. Ross, P.K. Bhattacharya, C.M. Marcus, In-vivo magnetic resonance imaging of hyperpolarized silicon particles, Nat. Nanotechnol. 8 (2013) 363-368. https://doi.org/10.1038/nnano.2013.65.
[57] R. Lockwood, Z. Yang, R. Sammynaiken, J.G.C. Veinot, A. Meldrum, Light-Induced Evolution of Silicon Quantum Dot Surface Chemistry – Implications for Photoluminescence, Sensing, and Reactivity, Chem. Mater. 26 (2014) 5467-5474. https://doi.org/10.1021/cm5008125.
[58] J.P King, K. Jeong, C.C. Vassiliou, C.S. Shin, R.H. Page, C.E. Avalos, H.J. Wang, A. Pines, Room-temperature in situ nuclear spin hyperpolarization from optically pumped nitrogen vacancy centres in diamond, Nat. Comm. 6 (2015) 8965. https://doi.org/10.1038/ncomms9965.
[59] M. Dasog, Z. Yang, S. Regli, T.M. Atkins, A. Faramus, M.P. Singh, E. Muthuswamy, S.M. Kauzlarich, R.D. Tilley, J.G.C. Veinot, Chemical insight into the origin of red and blue photoluminescence arising from freestanding silicon nanocrystals, ACS Nano 7 (2013), 2676-2685. https://doi.org/10.1021/nn4000644.
[60] J.L Pitters, P.G Piva, X. Tong, R.A. Wolkov, Reversible Passivation of Silicon Dangling Bonds with the Stable Radical TEMPO, Nano Lett. 3 (2003) 1431-1435. https://doi.org/10.1021/nl034258+.
[61] Z. Yang, C.M. Gonzalez, T.K. Purkait, M. Iqbal, A. Meldrum, J.G.C. Veinot, Radical Initiated Hydrosilylation on Silicon Nanocrystal Surfaces: An Evaluation of Functional Group Tolerance and Mechanistic Study, Langmuir 31 (2015) 10540-10548. https://doi.org/10.1021/acs.langmuir.5b02307.
[62] J.W. Aptekar, M.C. Cassidy, A.C. Johnson, R.A. Barton, M. Lee, A.C. Ogier, C. Vo, M.N. Anahtar, Y. Ren, S.N. Bhatia, C. Ramanathan, D.G. Cory, A.L. Hill, R.W. Mair, M.S. Rosen, R.L. Walsworth, C.M. Marcus, Silicon nanoparticles as hyperpolarized magnetic resonance imaging agents, ACS Nano 3 (2009) 4003-4008. https://doi.org/10.1021/nn900996p.
[63] A.V. Kessenikh, V.I. Lushchikov, A.A. Manenkov, Y.V. Taran, Proton polarization in irradiated polyethylenes, Sov. Phys. Solid State 5 (1963) 321-329.

[64] D.S. Wollan, Dynamic Nuclear-Polarization with Inhomogeneously Broadened ESR Line. 1. Theory, Phys. Rev. B 13 (1976) 3671-3685.
[65] D.S. Wollan, Dynamic Nuclear-Polarization with an Inhomogeneously Broadened ESR Line. 2. Experiment, Phys. Rev. B 13 (1976) 3686-3696.
[66] A. Abragam, Principles of Nuclear Magnetic Resonance, Oxford University Press: New York, 1961.
[67] C.P. Slichter, Principles of Magnetic Resonance, Harper & Row: New York, 1963.
[68] Y.P. Varshni, Temperature dependence of the energy gap in semiconductors, Physica 34 (1967) 149-154. https://doi.org/10.1016/0031-8914(67)90062-6.
[69] R. Sinelnikov, M. Dasog, J. Beamish, A. Meldrum, J.G.C. Veinot, Revisiting an Ongoing Debate: What Role Do Surface Groups Play in Silicon Nanocrystsal Photoluminescence?, ACS Photonics 4 (2017) 1920-1929. https://doi.org/10.1021/acsphotonics.7b00102.
[70] J.J. Wittmann, M. Eckardt, W. Harneit, B. Corzilius, Electron-driven spin diffusion supports crossing the diffusion barrier in MAS DNP, Phys. Chem. Chem. Phys. 20 (2018) 11418-11429. https://doi.org/10.1039/C8CP00265G.
[71] A.C. Pinon, J. Schlagnitweit, P. Berruyer, A.J. Rossini, M. Lelli, E. Socie, M. Tang, T. Pham, A. Lesage, S. Schantz, L. Emsley, Mesauring Nano- to Microstructures from Relayed Dynamic Nuclear Polarization NMR, J. Phys. Chem. C 121 (2017) 15993-16005. https://doi.org/10.1021/acs.jpcc.7b04438.
[72] S. Björgvinsdóttir, B.J. Walder, A.C. Pinon, L. Emsley, Bulk Nuclear Hyperpolarization of Inorganic Solids by Relay from the Surface. J. Am. Chem. Soc. 140 (2018) 7946-7951. https://doi.org/10.1021/jacs.8b03883.
[73] M. Matti Maricq, J.W. Waugh, NMR in rotating solids, J. Chem. Phys. 70 (1979) 3300-3316. https://doi.org/10.1063/1.437915.
[74] R. Rogawski, I.V. Sergeyev, Y. Zhang, T.H. Tran, Y. Li, L. Tong, A.E. McDermott, NMR Signal Quenching from Bound Biradical Affinity Reagents in DNP Samples, J. Phys. Chem. B 121 (2017) 10770-10781. https://doi.org/10.1021/acs.jpcb.7b08274.